



HAL
open science

Unraveling assemblage of microbial community dwelling in Dabaoshan As/Pb/Zn mine-impacted area: A typical mountain mining area of South China

Jian-Li Liu, Jun Yao, Ruofei Li, Houquan Liu, Jun-Jie Zhu, Geoffrey Sunahara, Robert Duran

► To cite this version:

Jian-Li Liu, Jun Yao, Ruofei Li, Houquan Liu, Jun-Jie Zhu, et al.. Unraveling assemblage of microbial community dwelling in Dabaoshan As/Pb/Zn mine-impacted area: A typical mountain mining area of South China. *Science of the Total Environment*, 2024, 912, pp.168850. 10.1016/j.scitotenv.2023.168850 . hal-04355237

HAL Id: hal-04355237

<https://univ-pau.hal.science/hal-04355237>

Submitted on 25 Mar 2024

HAL is a multi-disciplinary open access archive for the deposit and dissemination of scientific research documents, whether they are published or not. The documents may come from teaching and research institutions in France or abroad, or from public or private research centers.

L'archive ouverte pluridisciplinaire **HAL**, est destinée au dépôt et à la diffusion de documents scientifiques de niveau recherche, publiés ou non, émanant des établissements d'enseignement et de recherche français ou étrangers, des laboratoires publics ou privés.

1 Unraveling assemblage of microbial community dwelling in Dabaoshan
2 As/Pb/Zn mine-impacted area: A typical mountain mining area of South China

3
4 Jian-li Liu ^{a,*}, Jun Yao ^a, Ruofei Li ^a, Houquan Liu ^a, Jun-jie Zhu ^a,
5 Geoffrey Sunahara ^{a,b}, Robert Duran ^{a,c}

6
7 ^a School of Water Resources and Environment and Research Center of Environmental
8 Science and Engineering, Sino-Hungarian Joint Laboratory of Environmental
9 Science and Health, Beijing Key Laboratory of Water Resources & Environmental
10 Engineering, China University of Geosciences (Beijing), 29 Xueyuan Road,
11 Haidian District, 100083 Beijing, China

12 ^b Department of Natural Resource Sciences, McGill University, Montreal, Quebec,
13 H9X3V9, Canada

14 ^c Université de Pau et des Pays de l'Adour/E2S UPPA, IPREM UMR CNRS 5254, BP
15 1155, 64013 Pau Cedex, France

16
17 Submitted to: *Science of the Total Environment*

18 Word count: 4910 (excluding Abstract, References, and figure and table captions)

19 Figures: 6

20
21 * Corresponding Author. School of Water Resource and Environment
22 Engineering, China University of Geosciences (Beijing), 29 Xueyuan Road,
23 Haidian District, 100083 Beijing, China, E-mail: lj12489@cugb.edu.cn (J. Yao),
24 Tel: +86-10-82321958

26 **Abstract**

27 Microbial community assemblage includes microorganisms from the three domains
28 including Bacteria, Archaea, and Eukarya (Fungi), which play a crucial role in geochemical
29 cycles of metal(loid)s in mine tailings. Mine tailings harbor vast proportions of metal(loid)s,
30 representing a unique source of co-contamination of metal(loid)s that threaten the
31 environment. The elucidation of the assembly patterns of microbial communities in
32 mining-impacted ecospheres has received little attention. To decipher the microbial
33 community assembly processes, the microbial communities from the five sites of the
34 Dabaoshan mine-impacted area were profiled by the MiSeq sequencing of 16S rRNA
35 (Bacteria and Archaea) genes and internal transcribed spacers (Fungi). Results indicated that
36 the coexistence of 31 bacterial, 10 fungal, and 3 archaeal phyla, were mainly dominated by
37 *Mucilaginibacter*, *Cladophialophora*, and *Candidatus Nitrosotalea*, respectively. The
38 distribution of microorganisms was controlled by deterministic processes. The combination
39 of Cu, Pb, and Sb was the main factor explaining the structure of microbial communities.
40 Functional predicting analysis of bacteria and archaea based on the phylogenetic
41 investigation of communities by reconstruction of unobserved states analyses revealed that
42 the metabolic pathways related to arsenite transporter, arsenate reductase, and Fe-S cluster
43 were important for metal detoxification. Furthermore, the ecological guilds (pathogens,
44 symbiotrophs, and saprotrophs) of fungal communities explained 44.5% of functional
45 prediction. In addition, metal-induced oxidative stress may be alleviated by antioxidant
46 enzymes of fungi communities, such as catalase. Such information provides new insights into
47 the microbial assembly rules in co-contaminated sites.

48 **Keywords:** Assembly process; Mine-impacted ecospheres; Co-occurrence network;
49 Potential functional metabolism; Keystone taxa

50

51 **1. Introduction**

52 Sustainable environmental protection for non-ferrous mining wastes is vital for
53 the development of the national economy, industry, science, and technology. The
54 annual discharge of non-ferrous mining and smelting slag in the world exceeds 10
55 billion tons, which are open-air stacked in mine tailing dams (Wang *et al.*, 2017). The
56 content of metal(loid)s in non-ferrous tailings accounts for 30% - 90% of total
57 industrial discharges, and flotation reagents were three times more enriched than
58 pesticides in agricultural fields (Liu *et al.*, 2018; Zhang *et al.*, 2020). Such large
59 quantities of tailings containing toxic, hardly decomposed, and complex multiple
60 contaminants have seriously threatened food security and ecological security
61 (Alakangas *et al.*, 2010; Liu *et al.*, 2022a; Zhu *et al.*, 2018). Complexation between
62 metals and organic flotation reagents can accelerate the migration and transformation
63 of metals, as well as inhibit the degradation of flotation reagents (Zhang *et al.*, 2020;
64 Zhu *et al.*, 2018). Furthermore, exposure to toxicants in anthropogenic tailing dams by
65 drinking the contaminated water, ingestions of soil and food grown on the waste, and
66 dust inhalation could lead to dire consequences for human health (Hudson-Edwards,
67 2016; Torres *et al.*, 2018; Wang *et al.*, 2017).

68 Arsenic (As) bearing minerals are ubiquitous in tailings, including sulfides,
69 sulfosalts, arsenates, and arsenites (Giloteaux *et al.*, 2013). Arsenic has been listed as
70 a suspected carcinogen by the International Agency for Research on Cancer, which is
71 an agency of the World Health Organization. Additionally, the United States
72 Environmental Protection Agency and the United Nations Environment Programme
73 also recognize arsenic as a hazardous substance with potential carcinogenic properties.
74 Arsenic, regarded as an environmental threat for all types of organisms, could induce
75 cancers of the skin, lung, liver, and bladder among other tissues (Speer *et al.*, 2023).

76 Besides arsenic, elevated concentrations of associated metal(loid)s, such as copper
77 (Cu), lead (Pb), and zinc (Zn), are frequently found in or around mine tailings
78 worldwide (Hudson-Edwards, 2016).

79 Microorganisms (including Bacteria, Archaea, and Fungi) are important in the
80 transformation of metal(loid)s ensuring the functions that sustain ecosystems. Bacteria
81 are the dominant tailing-associated microorganisms (> 97%), followed by Archaea
82 (0.26% - 2.75%), and Eukarya (0.21% - 0.11%) (Liu *et al.*, 2023). The distribution
83 and composition of microorganisms can be driven by the spatial-temporal
84 heterogeneity of geochemical factors, climate, and temperature (Liang *et al.*, 2020; Yi
85 *et al.*, 2022). However, most studies have only focused on a single microbial
86 component, i.e., bacteria (Liu *et al.*, 2019a; Sun *et al.*, 2018), fungi (Liu *et al.*, 2022b;
87 Suting and Olivia Devi, 2021), or archaea (Chen *et al.*, 2021; Mendez-Garcia *et al.*,
88 2015). Bacterial, fungal, and archaeal communities can contribute to the
89 transformation of metal(loid) speciations and the degradation of flotation reagents in
90 the co-contamination nonferrous mine environment. Intrinsic linkages between
91 assembly processes and co-occurrences of bacteria, fungi, and archaea could facilitate
92 the management of microorganisms for better provision of ecosystem services.
93 However, to our knowledge, the co-occurrence of overall microbial assemblages
94 including bacterial, fungal, and archaeal communities in tailings has not been well
95 investigated.

96 To address this research gap, a study was conducted at a nonferrous mine tailing
97 site with As/Pb/Zn co-contaminated in a Dabaoshan mine-impacted area (see
98 Supplementary Information Fig. S1 and Table S1). We hypothesize here that: (1) the
99 assembly processes of bacterial, fungal, and archaeal communities are influenced by
100 various factors, including both biotic and abiotic elements, and (2) microbiological

101 communities with lower levels of species richness show greater linkages between
102 species. We analyzed the samples collected from the Dabaoshan As/Pb/Zn
103 mine-impacted area in a typical mountain mining area of South China. The objectives
104 of this study were to (1) evaluate the diversity, structure, and composition of bacterial,
105 fungal, and archaeal taxa in tailings; (2) reveal the ecological assembly processes and
106 co-occurrence patterns of the three domain taxa under the long-term metal(loid)s
107 co-contamination; and (3) explore the potential functional metabolism of taxa, which
108 could be used for the management of microbial resources. This study provides new
109 insights for studying community ecology, predicting responses to environmental
110 changes, and designing strategies for microorganism management and site restoration.

111 **2. Materials and methods**

112 2.1 Site description, sampling, and physical-chemical analyses

113 The Dabaoshan mining area is located in the northern Guangdong province
114 (southern China) and Lingnan mountain region with a hilly landform (24°30'01" -
115 24°35'26" N, 113°41'53" - 113°46'40" E, Fig. S1). The Dabaoshan mine, a typical
116 mountainous mining area, is the largest in South China (Wang *et al.*, 2019). It is a
117 large polymetallic mine composed mainly of Fe and Cu. It has been mined
118 extensively since the 1970s, and most of the metal ores are S-containing ores such as
119 pyrite, pyrrhotite, and chalcopyrite, which are important for the generation of acid
120 mine drainage (Bao *et al.*, 2018). The upper part of the polymetallic deposit was a
121 weathered and leached limonite, the middle part was layered siderite, and the lower
122 part was Cu, Pb, Zn, Fe, and S deposits, and porphyry Mb and Mb polymetallic
123 deposits (Luo *et al.*, 2021). The tailings site had been used for open storage of Pb-Zn
124 or Fe smelting slag for almost 30 years and was abandoned for almost 20 years. The
125 total amount of various solid wastes is over 9 million tons.

126 The sampling area covers a total surface area of 0.47 ha (Fig. S1). This area was
127 selected based on previous physical-chemical characterization studies (Zhang *et al.*,
128 2019), and has been undergoing natural attenuation for almost 20 years. The sampling
129 area was divided into five general sub-areas, which were divided along the directions
130 of the surrounding LiWu river (Fig. S1) and showed different physical-chemical
131 properties characteristics (Table S1). Due to the irregular terrain with high
132 heterogeneity of tailings, a random sampling strategy was adopted collecting
133 composite samples by nested sampling within a site. Composite samples using a
134 nested sampling design within a site accounted for environmental heterogeneity and
135 were reasonably reliable for the evaluation of the microbial diversity variation at a
136 small scale (Liu *et al.*, 2019).

137 For each sub-area, 13 samples were collected in December 2021 based on a
138 squared-figure sampling design. Samples were then combined and homogenized to
139 produce a composite sample to evaluate variations of bacteria, fungi, and archaea
140 communities. A total of five composite samples were finally harvested after field
141 sampling. All composite samples were immediately kept on ice (at 4°C) and delivered
142 to the China University of Geosciences (Beijing) within 48 h of sampling. Samples
143 for physical-chemical analysis were air-dried and sieved at 100-mesh size (0.149 mm,
144 US standard).

145 The detection of pH was done following the procedure of the China National
146 Agricultural Technology Extension Center (2006). After digestion in a microwave
147 with HNO₃-HCl-HF (5:3:2, v/v/v, GR), the concentrations of metal(loid)s were
148 measured by inductively coupled plasma-mass spectrometry (ICP-MS). More detailed
149 information for the measurements of pH and metal(loid)s concentrations was
150 previously described by Liu *et al.* (2021). The mineralogical composition of the

151 sample was determined using a scanning electron microscope (SEM) and energy
152 dispersive spectroscopy (EDS) spectrometer analysis, combined with phase analysis
153 of X-ray diffraction (XRD) and X-ray fluorescence (XRF). For microorganism
154 analysis, samples from each site were stored at -80 °C for further DNA extraction and
155 Miseq sequencing.

156 2.2 Amplification, MiSeq sequencing, and data processing

157 Total genomic DNA was extracted from ~ 10.0 g of each tailing sample using a
158 FastDNA® spin kit for soil (MP, Biomedicals, USA). The extracted DNA was
159 subjected to PCR amplification using the primer sets of: 1) ArBa515F
160 (GTGCCAGCMGCCGCGGTAA) and 806R (GGACTACHVGGGTWTCTAAT),
161 targeting the V3-V4 region of bacterial 16S rRNA gene (Liu *et al.*, 2023); 2) ITS1-F
162 (CTTGGTCATTTAGAGGAAGTAA) and ITS2-R
163 (GCTGCGTTCTTCATCGATGC), targeting the fungal genomic ITS region (Liu *et*
164 *al.*, 2022c); 3) 524F10extF (TGYCAGCCGCGCGGTAA) and Arch958RmodR
165 (YCCGGCGTTGAVTCCAATT), targeting the V3-V4 region of archaeal genomic
166 gene (Yi *et al.*, 2019). Polymerase chain reaction (PCR) reaction (20 µL) was carried
167 out containing 10 µL of 2×Pro Taq, 0.8 µL of forward/reverse primers (5 µM), 10
168 ng/µL of extracted template DNA, and double-distilled water. The PCR reaction was
169 performed on an ABI GeneAmp® 9700 Thermal Cycler with the procedures: initial
170 denaturation (3 min at 95°C), followed by 27 cycles of 30 s at 95°C, annealing 30 s
171 (at 55°C for bacteria, 55°C for archaea, and 50°C for fungi), and extension (45 s at
172 72°C), and a final extension (10 min at 72°C). This reaction was carried out (in
173 triplicate) for each composite sample, and then these samples were mixed into a new
174 PCR composite sample for sequencing. Sequencing was conducted on an Illumina
175 MiSeq platform at Majorbio Bio-Pharm Technology Co., Ltd (Shanghai, China).

176 The acquired sequences were filtered, and chimeric sequences were removed
177 using the USEARCH7-uparse clustering algorithm. Sequences were then split into
178 operational taxonomic units (OTUs) at a 97% similarity level according to 70%
179 classification confidence as previously described (Mamet *et al.*, 2017; Liu *et al.*,
180 2019a). All raw data were trimmed and filtered using fastp software (v0.19.4) by
181 filtering the reads below 50bp and reads with nitrogenous base. The fast length
182 adjustment of short reads (FLASH) software was used for merging the paired-end
183 reads of raw sequences. Sequences of bacterial/archaeal, and fungal were assigned to
184 taxonomic based on the taxonomy database of silva138/16s and unite8.0/its_fungi,
185 respectively. The sequence read archive accession number for the sequences is
186 SUB13926409.

187 2.4 Statistical analyses

188 To determine the differences in alpha-diversities of bacterial, fungal, and
189 archaeal communities, analyses based on the Wilcoxon test were calculated using
190 OTUs tables resampled to a minimum number of sequences from each sample
191 (39,922 for bacteria, 72,629 for fungi, and 42,962 for archaea). In present study, $p <$
192 0.05 is considered statistically significant. To estimate the beta-diversity of bacterial,
193 fungal, and archaeal communities, non-metric multidimensional scaling (NMDS) was
194 conducted based on the Bray-Curtis dissimilarity algorithms. The Partial Mantel test
195 determined the correlations between compositional and environmental data based on
196 Euclidean distances (Sunagawa *et al.*, 2015). BIOENV analysis was used to determine
197 the combined effects of physical-chemical parameters on the distribution of microbial
198 communities. The incidence-based (Raup-Crick) dissimilarity indices (β_{RC}) were
199 computed to determine whether communities were stochastically or deterministically
200 assembled. The neutral community model was constructed to evaluate the

201 contribution of neutral processes in community structure as described by others
202 (Sloan *et al.*, 2006). The Levins' niche breadth index for meta-communities was
203 estimated to reveal the patterns of meta-communities sorting and dispersal limitation
204 and their adaptability to the contaminated tailings. A high breadth index for a given
205 community indicates its wide habitat niche breadth. The wider the species niche, the
206 species is less specialized and more metabolically flexible. Co-occurrence network
207 analyses of bacterial, fungal, and archaeal communities were conducted by Gephi
208 software (v0.9.2) using the Frucherman Reingold algorithm as described by others
209 (Han *et al.*, 2017). The degree of the node of the co-occurrence network was assessed
210 by the number of nodes connected directly to that node. The more lines on the node,
211 the higher the degree, which indicates the intensity of correlation between the species
212 and other species.

213 To predict the potential functions of bacterial and archaeal communities, the
214 Phylogenetic Investigation of Communities by Reconstruction of Unobserved States
215 (PICRUSt2) was used to reveal the functions encoded in communities based on the
216 MetaCyc database. The weighted nearest sequenced taxon index (NSTI) was
217 calculated to assess the accuracy of PICRUSt2 analysis (Langille *et al.*, 2013). Kyoto
218 Encyclopedia of Genes and Genomes (KEGG) databases (e-value cut-off 10^{-5}) were
219 used for functional annotation. Significant differences in KOs between bacterial and
220 archaeal communities were analyzed based on the independent samples *T*-test. To
221 identify different functional groups within fungal communities, a recently developed
222 open annotation tool (FunGuild, Fungi Functional Guild) was used for the assignment
223 of fungal communities (Nguyen *et al.*, 2016). Redundancy analysis was used to
224 examine the correlations between KOs/Guilds and physical-chemical parameters
225 based on a weighted normalized unifracs distance algorithm. All the analyses were

226 done using R software (v 3.4.1) unless otherwise stated.

227

228 **3. Results and discussion**

229 3.1 The morphological characteristics of main mineral grains

230 The pH in the five studied samples ranged from 4.03 to 6.56 (Table S1), being
231 higher than the reported abandoned tailings (Liu *et al.*, 2019b; Liu *et al.*, 2021).

232 Generally, the heavy mineral fractions have typical metal(loid) concentrations that are
233 one order of magnitude greater, indicating that the majority of the contaminants are
234 likely bonded to high-density phases (Tuhý *et al.*, 2020). The metal(loid)
235 concentration (mg/kg) in the mineral fractions were in the following ranges: As (from
236 2180 to 2810), Fe (72900 - 97900), Pb (2800 - 4060), and Zn (1260 – 2220) (Table
237 S1). The levels of As, Fe, Pb, and Zn were from 1.36 to 17.98 times higher than the
238 soil environmental quality standard (GB15628-1995 and GB36600-2018).

239 Presumably, this contamination followed the release of metal(loid)s from smelter
240 tailing after > 30 years of abandonment (Alakangas *et al.*, 2010). According to the
241 ICP-MS analysis, the major potential toxicants were As, Pb, and Zn, resulting in
242 metal(loid) pollution in the Dabaoshan mine-impacted area. Correlation analysis
243 between metal(loid)s showed that As, Pb, Sb, and Zn had a significant positive
244 correlation with each other ($r = 0.878 - 0.978$; $p < 0.05$ or $p < 0.01$; Table S2) in the
245 studied sites. As well, Cr had a high correlation coefficient with Cu ($r = 0.916$; $p <$
246 0.05 ; Table S2). Results suggested that the elements had the same source, with similar
247 physical-chemical properties.

248 The XRD analysis indicated that samples were predominantly composed of quartz,
249 manganese copper oxide, Iwakiite, Celadonite, and Magnesium iron oxide (Fig. 1).

250 These five minerals, except quartz and Iwakiite, were often observed in the gangue
251 minerals. Some very complex minerals were also present as other minor phase forms
252 (Fig. 1). The presence of minor mineral phases may correspond to the
253 high-temperature amorphous and nanocrystalline phases produced during the smelting
254 and refining operations (Tuhý *et al.*, 2020; Zhu *et al.*, 2021). Representative
255 SEM-EDS images of the typical minerals are shown in Figure 1.

256 < Insert Fig. 1 >

257 The main minerals presented as irregular large particles and were composed of
258 various mineral grain aggregates. Moreover, the elemental composition (%) of tailings
259 samples consisted mainly of C (from 5.35 to 33.85), O (40.33 - 61.91), P (0.28 - 1.87),
260 Si (5.00 - 21.94), and S (0.15 - 2.11) (Table S3). The major metals were Al (6.21 -
261 17.84), As (0.11 - 1.36), Fe (1.00 - 38.96), Pb (0.16 - 4.47), and Zn (0.09 - 1.61), as
262 confirmed by XRF analysis (Table S4). It is likely that As and Zn participated in the
263 silicate structure (Zhu *et al.*, 2021). These results differed from data from samples
264 collected from Namibian mining/smelting-polluted soils (Tuhý *et al.*, 2020). Such
265 different mineral structures are probably due to different mining/smelting processes
266 adapted to the ore grade and the target extracted metals (Alakangas *et al.*, 2010; Liu *et*
267 *al.*, 2019a,2020; Tuhý *et al.*, 2020).

268 3.2 Characteristics of microbial communities

269 A total of 31 bacterial (1042 OTUs), 10 fungal (328 OTUs), and 3 archaeal (70
270 OTUs) phyla were obtained, which are consistent with earlier metagenomic analyses
271 showing that ~ 97% of microorganisms in tailings are assigned to bacteria (Liu *et al.*,
272 2023). The microbial diversity, relative abundance, and phylogenetic diversity
273 following down-weighting changed as follows: bacteria, fungi, and archaea (Fig. 2a).

274 The boneh and coverage estimates indicated that there would be no additional
275 observed OTUs for an additional level of sampling (coverage index > 99.87%). There
276 were differences in alpha-diversity indices (such as Shannon, Simpson, Chao1, ace,
277 and coverage) among bacterial, fungal, and archaeal communities ($p < 0.05$). The
278 distributions of OTUs based on BIOENV analysis appeared strongly driven by the
279 combination of pH, Pb, and Zn (bacteria OTUs, $r = 0.77$), Fe and Pb (fungi OTUs, $r =$
280 0.77), and Fe and Pb (archaea OTUs, $r = 0.37$) (Table S5). These results suggested
281 that physical-chemical parameters influenced the distribution of the OTUs from the
282 different microbial domains, which was consistent with other studies showing that the
283 dynamics of physical-chemical parameters as well as their complex combinations can
284 drive the microbial structure (Mamet *et al.*, 2017; Yi *et al.*, 2022).

285 < Insert Fig. 2 >

286 Among the 31 bacterial phyla, *Pseudomonadota* (25.3% - 38.6%), *Acidobacteriota*
287 (0.62% - 18.3%), and *Nitrospirota* (0.16% - 23.9%) dominated the tailings sites (Fig.
288 2b). *Pseudomonadota* and *Acidobacteriota* are common phyla in tailings from
289 different locations (Liu *et al.*, 2018). *Nitrospirota* includes only three valid and
290 published genera, harboring potentially dissimilatory sulfur metabolisms (Umezawa
291 *et al.*, 2020). In the fungal communities, *Ascomycota* and *Basidiomycota* accounted
292 for > 95.2% of the sequences across all tailings (Fig. 2c). These fungal phyla are
293 dominant in various environments, such as soil (Moussa *et al.*, 2017) and lead-zinc
294 tailings (Jia *et al.*, 2021). Archaeal communities were dominated by
295 *Thermoplasmatota* (56.6%) and *Crenarchaeota* (43.3%) phyla (Fig. 2d). Evidence
296 showed that the *Thermoplasmatota* accounted for 75.1%, while *Crenarchaeota* were
297 not represented in an acid mine drainage environment of France (Bruneel *et al.*, 2008;
298 Calum 2023). This is likely due to the different geological environment conditions

299 and tailings types. *Thermoplasmatota* and *Crenarchaeota*, which harbor aerobic
300 respiration and acid tolerance genes, could contribute to the indigenous microbial
301 genetic repertoire to expand into a new habitat (Brochier-Armanet *et al.*, 2008;
302 Sheridan *et al.*, 2022). Also, there are few studies on the composition and structure of
303 the archaeal communities in metal(loid) tailings. In the present study, most of the
304 sequences could not be identified for bacteria (54.2%), fungi (26.1%), and archaea
305 (44.4%) (Fig. 2b-d). The microbial identification described here was lower than that
306 reported for other tailings such as Sb-rich or multi-contaminated nonferrous
307 metal(loid) tailings dumps (Liu *et al.*, 2019b; Xiao *et al.*, 2016). Such observation
308 suggests that a vast microbial population in tailings remains under-exploited; their
309 exploration would benefit bioremediation and environmental management (Liu *et al.*,
310 2019a).

311 3.3 Potential processes governing the microbial assemblage

312 We also explored the microorganism taxonomic classifications and their relative
313 distributions in tailings. The NMDS ordination analysis based on Bray-Curtis
314 similarity distance assessed the beta-diversity of the bacterial, fungal, archaeal, and all
315 microbial communities in tailings (Fig. 3a-d). Bacterial and fungal communities were
316 only detected in four sampling sites except at the T2 site (Fig. 2b,c), and tailing sites
317 (T3 and T5) with a pH > 5 were compared to that < pH 5 (T1 and T4) (Fig. 3a,b).

318 < Insert Fig. 3 >

319 The pH plays a critical role in affecting the abundance and distribution of microbes
320 (Chen *et al.*, 2014). Unexpectedly, archaeal communities were detected in five sites,
321 including the T2 sampling site (Fig. 2d), which was distant from the other sites (Fig.
322 3c). Also, the distribution of bacterial and fungal communities was more similar to

323 each other than that of archaeal communities ($p = 0.018$, stress = 0.073, permutations
324 = 999; Fig. 3d). The environmental factors driving the relationships between the three
325 domains of life were examined based on Mantel test (Fig. 3b). Overall, the Cu, Pb,
326 and Sb contents were the major factors correlating with the abundance distribution of
327 bacteria, fungi, and archaea ($p < 0.05$; Fig. 3b), whereas the pH, Fe, and Zn contents
328 were not correlated ($p > 0.05$; Fig. 3b). Such observation probably reflects the
329 dissimilarity distribution of OTUs among the sites, suggesting that the microbial
330 composition exhibits habitat-specific patterns. This confirms the possibility that the
331 distribution and composition of microbial communities are changed by dynamic and
332 rapidly changing conditions, likely caused by anthropogenic activity-induced stresses,
333 temperature, oxygen, salinity, latitude, and seasonal changes (Cabral *et al.*, 2016;
334 Cravo-Laureau *et al.*, 2017; Giloteaux *et al.*, 2013; Pringault *et al.*, 2008).
335 Nevertheless, in natural environments, the composition and distribution of
336 microorganisms interact with both biotic and abiotic components (Cravo-Laureau *et*
337 *al.*, 2017). Network analysis showing the co-occurrence abundance of members of the
338 three domains of life indicated that *Mucilaginibacter*, *Cladophialophora*, and
339 *Candidatus Nitrosotalea* were found as Specialists, being the main contributing
340 genera (Fig. 4).

341 < Insert Fig. 4 >

342 It is also worth mentioning that co-occurrence analysis identified the rare taxa of
343 *Mucilaginibacter* and *Cladophialophora* (< 1.79%; Fig. 2b,c) identified as Specialist,
344 corresponding to keystone taxa organizing the microbial assemblage in tailings.
345 Recent studies explored that keystone taxa have a pivotal role in driving microbial
346 structure and functioning (Banerjee *et al.*, 2018; Herren and McMahon, 2018). Both
347 *Mucilaginibacter* and *Cladophialophora* contain members resistant to potential toxic

348 metal(loid)s and can adapt to contaminated environments (Taleski *et al.*, 2020;
349 Vasconcelos *et al.*, 2021). Additionally, the dominated archaeal members of
350 *Candidatus Nitrosotalea* (16.2% - 70.6%; Fig. 2d) were also affiliated with keystone
351 taxa. *Candidatus Nitrosotalea*, an obligate acidophilic ammonia oxidizer, contains
352 genes encoding predicted potential pH homeostasis mechanisms (Lehtovirta-Morley
353 *et al.*, 2016). Thus, our results revealed that both rare and abundant taxa contribute to
354 ecosystem stability and function, which is consistent with previous reports in coastal
355 systems (Hugoni *et al.*, 2013).

356 To define the relative importance of deterministic and stochastic processes in
357 shaping microbial community structure incidence-based (Raup-Crick) beta-diversity
358 (β_{RC}) tests were conducted (Fig. 5a). The mean values of β_{RC} were close to |1| for the
359 three domains of life, indicating deterministic processes control microbial
360 assemblages. For the bacterial communities, the deterministic processes favored
361 dissimilar communities, whereas for archaeal and fungal communities, the
362 deterministic assemblage processes produced more similar communities than
363 expected by chance. However, neutral community model analysis revealed a
364 negligible degree of stochastic processes (Fig. 5b and Fig. S2), confirming its minor
365 role in the assembly of microbial communities. In addition, fungal communities
366 demonstrated wider niche breadths than the archaeal and bacterial communities (Fig.
367 5c), indicating higher fungal metabolic flexibility and redundancy. A possible
368 explanation is that the Dabaoshan mine-impacted area is a unique habitat due to
369 long-term abandonment. This As, Pb, and Zn co-contamination resulted in specific
370 environmental filtering that influences the niche breadth such as abiotic conditions,
371 biotic interactions, or geographical ranges (Malard *et al.*, 2021).

372 < Insert Fig. 5 >

373 3.4 Potential metabolism and predicted functions

374 3.4.1 Metal-related functions of bacterial and archaeal communities

375 The bacterial and archaeal metabolic potentials were inferred by PICRUSt2
376 analysis (Fig. S3). The obtained NSTI values for both bacterial and archaeal
377 communities were low (0.00 - 0.36; Table S6), and the mean fraction of sequences
378 used in PICRUSt2 prediction were > 99.89% (Table S6), indicating that the prediction
379 was accurate (Douglas *et al.*, 2019; Langille *et al.*, 2013). The extremely high
380 concentrations of As, Fe, Pb, and Zn in the studied tailings likely enriched the
381 abundance of metal-resistance genes during the long term (Table S1) compared to
382 short-term exposures (Liu *et al.*, 2021). Among the 6779 (for bacterial community)
383 and 3145 (for archaeal community) KOs, 23 metal-related KOs were shared for
384 bacterial and archaeal communities (Fig. S3; Table S7 and S8). Relative abundances
385 of KOs were related to arsenite transporter (K03325), arsenate reductase (K03741),
386 and Fe-S cluster assembly proteins (K09013-9015) differed between bacterial and
387 archaeal communities ($p < 0.05$; Fig. 6a).

388 < Insert Fig. 6 >

389 It was noteworthy that the detected arsenate reductase and arsenite transporter could
390 reduce As^{5+} to As^{3+} to be retained in the bacterial cell, released into the air, or both
391 (Rahman *et al.*, 2021). Although the expression of KO genes related to arsenate
392 respiratory reductase (*arr*) may not be strictly anaerobic (Jia *et al.*, 2014), the KOs
393 were not revealed by PICRUSt2 here (Fig. S3). Microorganisms harboring *arr* genes
394 can use arsenate as a terminal electron acceptor for respiration in cell periplasm
395 (Bhattacharjee and Rosen, 2000). Thus, a proportion of microorganisms should be
396 active for arsenic detoxification in the studied sites. The KOs related to Fe-S cluster

397 assembly protein were dominant for archaeal communities. The Fe-S cluster assembly
398 could traffic the toxic iron and sulfide to the target metalloproteins to maintain the
399 Fe-S homeostasis (Chahal *et al.*, 2009). The shared KOs related to Co-Zn-Cd efflux
400 system protein (K16264) and arsenite/tail-anchored protein-transporting ATPase
401 (K01551) were also detected (Tables S7 and S8). The arsenite/tail-anchored
402 protein-transporting ATPase could couple with arsenic pump membrane protein for
403 the cellular expulsion of arsenite or antimonite (Bhattacharjee and Rosen, 2000).

404 Additionally, specific KOs between bacterial and archaeal communities were also
405 detected (Fig. S3 and Table S7). The distinct distribution of these predicted functional
406 pathways was strongly correlated with As, Fe, and Pb contents ($r = 0.98$; Fig. 6b,c).
407 Additional contamination, whether organic or metallic/metalloid, could modify the
408 composition and function of microorganisms in natural habitats (Ning *et al.*, 2020;
409 Mendez-Garcia *et al.*, 2015). For bacterial taxa, specific KOs related to the
410 arsenate/arsenite/antimonite responsive transcriptional repressor (K03892), F-type
411 H⁺-transporting ATPase subunit *b* (K02108 - K02115), Fe³⁺ transporters (K02010,
412 K02011, and K02012), and metal efflux systems (K15726, K07787) showed high
413 relative abundance (Fig. S3a). The KOs related to Fe³⁺ transport and metal efflux
414 could mediate resistance to Co²⁺, Zn²⁺, Cd²⁺, and Fe³⁺ and function as a cation/proton
415 antiport for the removal of cellular cations (Cabral *et al.*, 2016). Given the presence of
416 several metal-efflux pumps and metal-regulated gene expression in tailings, these
417 processes may be crucial in the detoxification of metals (Maynaud *et al.*, 2014; Ren *et*
418 *al.*, 2017). For archaeal taxa, the dominant KOs related to arsenite/tail-anchored
419 protein-transporting ATPase (K01551) were specific to the Dabaoshan As/Pb/Zn
420 mine-impacted area (Fig. S3b and Table S8). To adapt to the extreme tailings
421 environment, microorganisms harbored specific functions known as essential for the

422 biogeochemical cycling and biodegradation of pollutants (Cravo-Laureau *et al.*,
423 2017).

424 3.4.2 Functional prediction of fungal communities

425 We assigned fungal OTUs into specific ecological guilds based on FUNGuild
426 (Fig. S4a). Three ecological guilds (pathogens, symbiotrophs, and saprotrophs)
427 accounted for ~ 44.5% of all the fungal OTUs (Fig. S4a). It was surprising to detect
428 relatively high numbers of animal pathogens and soil saprotrophs in the studied
429 tailings (Fig. S4a). The animal pathogens always showed a high abundance in the
430 forest or soil system with different degrees of residency: permanent, periodic,
431 transient, and incidental (Samaddar *et al.*, 2021). The relatively high abundance of
432 animal pathogens seen here was likely introduced anthropogenically or after surface
433 runoff or aerial disposition. Soil saprotrophs were the key fungi in the decomposition
434 of recalcitrant organic C, conducting biogeochemical cycles of key nutrients (Liu *et*
435 *al.*, 2022c). Correlation analyses using the geochemical parameters showed that the
436 distribution of functional fungal guilds, such as soil saprotroph was correlated with
437 concentrations of As, Fe, and Pb ($p < 0.05$; Fig. S4c). Such observation further
438 supports that deterministic processes are the most important process driving fungal
439 distributions in tailings. Also, the newly updated PICRUST2 software was utilized to
440 explore the functional features of fungal communities (Fig. S4b). The relevant
441 antioxidant enzymes, such as catalase, glucose-6-phosphate dehydrogenase,
442 glutathione reductase, peroxidase, and superoxide dismutase were selected from the
443 functional predictions (Fig. S4b and Table S9). These metal antioxidant enzymes can
444 mitigate the membrane lipid peroxidation damage caused by metal stress, and
445 maintain the community stability (Azevedo *et al.*, 2007; Garg and Kaur, 2013). These
446 antioxidant enzymes could enhance the coping mechanism to metal-induced oxidative

447 stress in As/Pb/Zn contamination tailings. Thus, the functional fungal taxa adapting to
448 metal stress may be potential candidates for tailings restoration. Restoration based on
449 indigenous sulfate-reducing bacteria consortium has been applied to the maintenance
450 and stabilization of metal(loid)s in tailings (Liu *et al.*, 2019a; Li *et al.*, 2022).
451 Microorganisms inhabiting mine tailings require specific metabolic strategies for their
452 survival and may hold potential resources for future pollution cleanup strategies.
453 Effective in situ bioremediation will rely on an in-depth understanding of the function
454 of the bacterial communities, especially the abundant and metabolically active
455 phylotypes.

456 **5. Conclusions**

457 The present study provides new insight into the co-occurrence patterns of
458 bacteria, fungi, and archaea communities in co-contaminated typical metal(loid)
459 tailings after 20 years of abandonment. The combined mineralogy analyses revealed
460 that As, Pb, and Zn were the major toxicants. The microbial distribution patterns
461 indicated that the assemblages of bacterial, fungal, and archaeal taxa were influenced
462 by the metal(loid)s (including Cu, Pb, and Sb), which suggests that deterministic
463 processes play a key role in shaping microbial community assemblages. The
464 microbial community arranges around keystone taxa such as members of
465 *Mucilaginibacter*, *Cladophialophora*, and *Candidatus Nitrosotalea* genera. The
466 PICRUSt analysis showed that specific functional KOs attested to the distinct roles of
467 bacteria and archaea communities prevailing in the metal detoxification of tailings,
468 such as As⁵⁺. The relevant antioxidant enzymes of fungi taxa (catalase and glutathione
469 reductase) could relieve metal-induced oxidative stress. To the best of our knowledge,
470 the present study provides, for the first time, new insight into how microbial
471 communities (including Bacteria, Archaea, and Fungi) respond to typical As/Pb/Zn

472 mine tailings. Such emerging technologies are applicable for the future restoration of
473 soils co-contaminated with metal(loid)s from mine tailings.

474

475 **Credit author statement**

476 **Jian-li Liu**: Samples collecting, Data Analysis, Writing - original draft; **Jun Yao**:
477 Writing-Reviewing and Editing, and Validation; **Ruofei Li**: Samples collecting;
478 **Houquan Liu** and **Jun-jie Zhu**: Morphological analysis of main mineral grains;
479 **Geoffrey Sunahara** and **Robert Duran**: Writing - Review & Editing.

480

481 **Declaration of competing interest**

482 The authors declare that no conflict of financial interest or personal relationships
483 exists in the submission of this manuscript.

484 **Data availability**

485 Data will be made available on request.

486

487 **Acknowledgments**

488 This work is supported in part by grants from projects of the Major National R &
489 D Projects For the Chinese Ministry of Science and Technology (2020YFC1807600),
490 and the National Natural Science Foundation of China (42007289), the 111 Project
491 (B21017), the 1000-Talents Plan Project (WQ2017110423), and the Fundamental
492 Research Funds for the Central Universities (53200759777).

493

494 **Appendix A. Supporting information**

495 Supplementary data related to this article can be found on the website of *Science of*
496 *the Total Environment*.

497

498 **References**

- 499 Alakangas L., Ohlander B., Lundberg A., 2010. Estimation of temporal changes in oxidation
500 rates of sulphides in copper mine tailings at Laver, Northern Sweden. *Sci. Total Environ.*
501 408, 1386-1392. <https://doi.org/10.1016/j.scitotenv.2009.11.005>
- 502 Azevedo M.M., Carvalho A., Pascoal C., Rodrigues F., Cássio F., 2007. Responses of
503 antioxidant defenses to Cu and Zn stress in two aquatic fungi. *Sci Total Environ.*
504 377(2-3), 233-43. <https://doi.org/10.1016/j.scitotenv.2007.02.027>
- 505 Banerjee S., Schlaeppi K., van der Heijden, M.G.A., 2018. Keystone taxa as drivers of
506 microbiome structure and functioning. *Nat. Rev. Microbiol.* 16, 567-576.
507 <https://doi.org/10.1038/s41579-018-0024-1>
- 508 Bao Y., Guo C., Lu G., Yi X., Wang H., Dang Z., 2018. Role of microbial activity in Fe(III)
509 hydroxysulfate mineral transformations in an acid mine drainage-impacted site from the
510 Dabaoshan Mine. *Sci Total Environ.* 616-617, 647-657.
511 <https://doi.org/10.1016/j.scitotenv.2017.10.273>
- 512 Bhattacharjee H., Rosen B.P., 2000. Role of conserved histidine residues in metalloactivation
513 of the *ArsA* ATPase. *Biometals* 13, 281-288. <https://doi.org/10.1023/a:1009200215328>
- 514 Brochier-Armanet C., Boussau B., Gribaldo S. Forterre P., 2008. Mesophilic crenarchaeota:
515 Proposal for a third archaeal phylum, the *Thaumarchaeota*. *Nat. Rev. Microbiol.* 6,
516 245-252. <https://doi.org/10.1038/nrmicro1852>
- 517 Bruneel O., Pascault N., Egal M., Bancon-Montigny C., Goni-Urriza M.S., Elbaz-Poulichet F.,
518 Personné J.-C., Duran R., 2008. Archaeal diversity in a Fe-As rich acid mine drainage at
519 Carnoules (France). *Extremophiles* 12, 563-571.
520 <https://doi.org/10.1007/s00792-008-0160-z>
- 521 Cabral L., Júnior G.V.L., Pereira De Sousa S.T., Franco Dias A.C., Cadete L.L., Dini
522 Andreote F., Hess M., de Oliveira V.M., 2016. Anthropogenic impact on mangrove
523 sediments triggers differential responses in the heavy metals and antibiotic resistomes of
524 microbial communities. *Environ. Pollut.* 216, 460-469.
525 <https://doi.org/10.1016/j.envpol.2016.05.078>
- 526 Chahal H.K., Dai Y., Saini A., Ayala-Castro C., Outten F.W., 2009. The *SufBCD* Fe-S
527 scaffold complex interacts with *SufA* for Fe-S cluster transfer. *Biochemistry* 48,
528 10644-10653. <https://doi.org/10.1021/bi901518y>
- 529 Chen Y.T., Li J.T., Chen L.X., Hua Z.S., Huang L.N., Liu J., Xu B.B., Liao B., Shu W.S.,
530 2014. Biogeochemical processes governing natural pyrite oxidation and release of acid

531 metalliferous drainage. *Environ. Sci. Technol.* 48, 5537-5545.
532 <https://doi.org/10.1021/es500154z>

533 Chen Z., Liu W., Zhong X., Fei Y., He H., Ding K., Chao Y., Tang Y., Wang S., Qiu R., 2021.
534 Genome- and community-level interaction insights into the ecological role of archaea in
535 rare earth element mine drainage in South China. *Water Res.* 201, 117331.
536 <https://doi.org/10.1016/j.watres.2021.117331>

537 Cravo-Laureau C., Cagnon C., Lauga B., Duran R., 2017. *Microbial Ecotoxicology*. Springer
538 International Publishing, Switzerland. <https://doi.org/10.3389/fmicb.2020.01342>

539 Douglas G.M., Maffei V.J., Zaneveld J., Yurgel S.N., Brown J.R., Taylor C.M., Huttenhower
540 C., Langille M.G.I., 2019. PICRUSt2: an improved and extensible approach for
541 metagenome inference. *bioRxiv* <http://dx.doi.org/10.1101/672295>

542 Frenk S., Hadar Y., Minz D., 2018. Quality of irrigation water affects soil functionality and
543 bacterial community stability in response to heat disturbance. *Appl. Environ. Microbiol.*
544 84, e02087-17. <https://doi.org/10.1128/AEM.02087-17>

545 Garg N. and Kaur H., 2013. Response of antioxidant enzymes, phytochelatins and glutathione
546 production towards Cd and Zn stresses in *Cajanus cajan* (L.) Millsp. genotypes
547 colonized by arbuscular mycorrhizal fungi. *J. Agron. Crop Sci.* 199, 118-133.
548 <https://doi.org/10.1111/j.1439-037X.2012.00533.x>

549 Giloteaux L., Duran R., Casiot C., Bruneel O., Elbaz-Poulichet F., Goñi-Urriza M., 2013.
550 Three-year survey of sulfate-reducing bacteria community structure in Carnoulès acid
551 mine drainage (France), highly contaminated by arsenic. *FEMS Microbiol. Ecol.*
552 83,724-737. <https://doi.org/10.1111/1574-6941.12028>

553 Han Y., Wang J., Zhao Z, Chen J., Lu H., Liu G., 2017. Fishmeal application induces
554 antibiotic resistance gene propagation in mariculture sediment. *Environ. Sci. Technol.* 51,
555 10850-10860. <https://doi.org/10.1021/acs.est.7b02875>

556 Herren C.M. and McMahon K.D., 2018. Keystone taxa predict compositional change in
557 microbial communities. *Environ Microbiol.* 20, 2207-2217.
558 <https://doi.org/10.1111/1462-2920.14257>

559 Hudson-Edwards K., 2016. Tackling mine wastes. *Science* 352, 288-290.
560 <http://doi.org/10.1126/science.aaf3354>

561 Hugoni M., Taib N., Debroas D., Domaizon I., Dufournel I.J., Bronner G., Salter I., Agogué
562 H., Mary I., Galand P.E., 2013. Structure of the rare archaeal biosphere and seasonal
563 dynamics of active ecotypes in surface coastal waters. *PNAS* 110, 6004-6009.

564 <https://doi.org/10.1073/pnas.1216863110>

565 Jia T., Wang X., Guo T., Chai B., 2021. Litter decomposition of *Imperata cylindrica* in a
566 copper tailing areas with different restoration history: Fungal community dynamics and
567 driving factors. *Front. Microbiol.* 12, 780015.
568 <https://doi.org/10.3389/fmicb.2021.780015>

569 Jia Y., Huang H., Chen Z., Zhu Y., 2014. Arsenic uptake by rice is influenced by
570 microbe-mediated arsenic redox changes in the rhizosphere. *Environ. Sci. Technol.* 48,
571 1001-1007. <https://doi.org/10.1021/es403877s>

572 Langille M.G.I., Zaneveld J., Caporaso J.G., McDonald D., Knights D., Reyes J.A., Clemente
573 J.C., Burkepille D.E., Vega Thurber R.L., Knight R., Beiko R.G., Huttenhower C., 2013.
574 Predictive functional profiling of microbial communities using 16S rRNA marker gene
575 sequences. *Nat. Biotechnol.* 31, 814-821. <https://doi.org/10.1038/nbt.2676>

576 Latzel V., Allan E., Bortolini S.A., Colot V., Fischer M., Bossdorf O., 2013. Epigenetic
577 diversity increases the productivity and stability of plant populations. *Nat. Commun.* 4,
578 2875. <https://doi.org/10.1038/ncomms3875>

579 Lehtovirta-Morley L.E., Sayavedra-Soto L.A., Gallois N., Schouten S., Stein L.Y., Prosser
580 J.I., Nicola G.W., 2016. Identifying potential mechanisms enabling acidophily in the
581 ammonia-oxidizing archaeon "*Candidatus Nitrosotalea devanattera*." *Appl Environ*
582 *Microbiol.* 82, 2608-2619. <https://doi.org/10.1128/aem.04031-15>

583 Liang J., Liu J., Jia P., Yang T., Zeng Q., Zhang S., Liao B., Shu W., Li J., 2020. Novel
584 phosphate-solubilizing bacteria enhance soil phosphorus cycling following ecological
585 restoration of land degraded by mining. *ISME J.* 14, 1600-1613.
586 <https://doi.org/10.1038/s41396-020-0632-4>

587 Li M., Yao J., Sunahara G., Hawari J., Duran R., Liu J., Liu B., Cao Y., Pang W., Li H., Li Y.,
588 Ruan Z., 2022. Novel microbial consortia facilitate metalliferous immobilization in
589 non-ferrous metal(loid)s contaminated smelter soil: efficiency and mechanisms. *Environ*
590 *Pollut.* 15, 120042. <https://doi.org/10.1016/j.envpol.2022.120042>

591 Liu B., Yao J., Chen Z., Ma B., Liu J., Li H., Zhu X., Li M., Cao Y., Pang W., Zhao C.,
592 Mihucz V.G., Duran R., 2022a. Unraveling ecological risk of As/Sb and other
593 metal(loid)s and fungal community responses in As/Sb smelting-intensive zone: A
594 typical case study of Southwest China. *J. Clean. Prod.* 338, 130525.
595 <https://doi.org/10.1016/j.jclepro.2022.130525>

596 Liu B., Yao J., Ma B., Li S., Duran R., 2022b. Disentangling biogeographic and underlying
597 assembly patterns of fungal communities in metalliferous mining and smelting soils. *Sci.*

598 *Total Environ.* 845, 157151. <https://doi.org/10.1016/j.scitotenv.2022.157151>

599 Liu J., Yao J., Duran R., Mihucz V.G., Hudson-Edwards K.A., 2019a. Bacterial shifts during
600 in-situ mineralization bio-treatment to non-ferrous metal(loid) tailings. *Environ. Pollut.*
601 255, 113165. <https://doi.org/10.1016/j.envpol.2019.113165>

602 Liu J., Yao J., Wang F., Ni W., Liu X., Sunahara G., Duran R., Jordan G., Hudson-Edwards
603 K.A., Alakangas L., Solevic-Knudsen T., Zhu X., Zhang Y., Li Z., 2018. China's most
604 typical nonferrous organic-metal facilities own specific microbial communities. *Sci.*
605 *Rep-UK* 8, 12570-12580. <https://doi.org/10.1038/s41598-018-30519-1>

606 Liu J., Yao J., Wang F., Min N., Gu J., Li Z., Sunahara G., Duran R., Solevic-Knudsen T.,
607 Hudson-Edwards K.A., Alakangas L., 2019b. Bacterial diversity in typical abandoned
608 multi-contaminated nonferrous metal(loid) tailings during natural attenuation. *Environ.*
609 *Pollut.* 247, 98-107. <https://doi.org/10.1016/j.envpol.2018.12.045>

610 Liu J., Yao J., Zhou D., Liu B., Liu H., Li M., Zhao C., Sunahara G., Duran R., 2023.
611 Mining-related multi-resistance genes in sulfate-reducing bacteria treatment of typical
612 karst nonferrous metal(loid) mine tailings in China. *Environ. Sci. Pollut. R.* 30,
613 104753-104766. <https://doi.org/10.1007/s11356-023-29203-3>

614 Liu J., Yao J., Zhu X., Zhou D., Duran R., Mihucz V.G., Bashir S., Hudson-Edwards K.A.,
615 2021. Metagenomic exploration of multi-resistance genes linked to microbial attributes
616 in active nonferrous metal(loid) tailings. *Environ. Pollut.* 273, 115667.
617 <https://doi.org/10.1016/j.envpol.2020.115667>

618 Liu S., García-Palacios P., Tedersoo L., Guirado E., van der Heijden M.G.A., Wagg C., Chen
619 D., Wang Q., Wang J., Singh B.K., Delgado-Baquerizo M., 2022c. Phylotype diversity
620 within soil fungal functional groups drives ecosystem stability. *Nat. Ecol. Evol.* 6,
621 900-909. <https://doi.org/10.1038/s41559-022-01756-5>

622 **Lloyd C., 2023. Cultured microbial diversity of Parys mountain acidic site. PhD thesis.**
623 **School of Environmental and Natural Sciences, UK: Bangor University.**

624 Luo C., Routh J., Luo D., Wei L., Liu Y., 2021. Arsenic in the Pearl River Delta and its
625 related waterbody, South China: occurrence and sources, a review. *Geosci. Lett.* 8, 12.
626 <https://doi.org/10.1186/s40562-021-00185-9>

627 Malard L.A., Mod H.K., Guex N., Broennimann O., Yashiro E., Lara E., Mitchell E.A.,
628 Niculita-Hirzel H., Guisan A., 2021. Comparative analysis of diversity and
629 environmental niches of soil bacterial, archaeal, fungal and protist communities reveal
630 niche divergences along environmental gradients in the Alps. *Soil Biol. Biochem.* 169,
631 108674. <https://doi.org/10.1016/j.soilbio.2022.108674>

632 Mamet S.D., Lamb E.G., Piper C.L., Winsley T., Siciliano S.D., 2017. Archaea and bacteria
633 mediate the effects of native species root loss on fungi during plant invasion. *ISME J.* 11,
634 1261-1275. <https://doi.org/10.1038/ismej.2016.205>

635 Maynaud G., Brunel B., Yashiro E., Mergeay M., Cleyet-Marel J.C., Le Quéré A., 2014.
636 *CadA* of *Mesorhizobium metallidurans* isolated from a zinc-rich mining soil is a
637 P(IB-2)-type ATPase involved in cadmium and zinc resistance. *Res Microbiol.* 165,
638 175-89. <https://doi.org/10.1016/j.resmic.2014.02.001>

639 Mendez-Garcia C., Pelaez A. I., Mesa V., Sánchez J., Golyshina O.V., Ferrer M., 2015.
640 Microbial diversity and metabolic networks in acid mine drainage habitats. *Front.*
641 *Microbiol.* 6, 475. <https://doi.org/10.3389/fmicb.2015.00475>

642 Moussa T.A.A., Al-Zahrani H.S., Almaghrabi O.A., Abdelmoneim T.S., Fuller M.P., 2017.
643 Comparative metagenomics approaches to characterize the soil fungal communities of
644 western coastal region, Saudi Arabia. *PLOS ONE* 12, e0185096.
645 <https://doi.org/10.1371/journal.pone.0185096>

646 Nguyen N.H., Song Z., Bates S.T., Branco S., Tedersoo L., Menke J., Schilling J.S., Kennedy
647 P.G., 2016. FUNGuild: an open annotation tool for parsing fungal community datasets
648 by ecological guild. *Fungal Ecol.* 20, 241-248.
649 <https://doi.org/10.1016/j.funeco.2015.06.006>

650 Ning D., Yuan M., Wu L., Zhang Y., Guo X., Zhou X., Yang Y., Arkin A.P., Firestone M.K.,
651 Zhou J., 2020. A quantitative framework reveals ecological drivers of grassland
652 microbial community assembly in response to warming. *Nat. Commun.* 11, 4717.
653 <https://doi.org/10.1038/s41467-020-18560-z>

654 Rahman M.S., Hossain M.S., Saha S.K., Rahman S., Sonne C., Kim K., 2021. Homology
655 modeling and probable active site cavity prediction of uncharacterized arsenate reductase
656 in bacterial spp. *Appl. Biochem. Biotechnol.* 193, 3119-3135.
657 <https://doi.org/10.1007/s12010-020-03392-w>

658 Ren S., Li Q., Xie L., Xie J., 2017. Molecular mechanisms underlying the function diversity
659 of *ArsR* family metalloregulator. *Crit. Rev. Eukar. Gene.* 27, 19-35.
660 <https://doi.org/10.1615/critreveukaryotgeneexpr.2016018476>

661 Samaddar S., Karp D. S., Schmidt R., Devarajan N., McGarvey J.A., Pires A.F.A., Scow K.,
662 2021. Role of soil in the regulation of human and plant pathogens: soils' contributions to
663 people. *Phil. Trans. R. Soc. B* 376, 20200179. <https://doi.org/10.1098/rstb.2020.0179>

664 Sheridan P.O., Meng Y., Williams T.A., Gubry-Rangin C., 2022. Recovery of
665 *Lutacidiplasmatales* archaeal order genomes suggests convergent evolution in

666 *Thermoplasmatota*. *Nat. Commun* 13, 4110. <https://doi.org/10.1038/s41467-022-31847-7>

667 Sloan W.T., Lunn M., Woodcock S., Head I.M., Nee S., Curtis T.P., 2006. Quantifying the
668 roles of immigration and chance in shaping prokaryote community structure. *Environ.*
669 *Microbiol.* 8, 732-740. <https://doi.org/10.1111/j.1462-2920.2005.00956.x>

670 Speer R.M., Zhou X., Volk L.B., Liu K.J., Hudson L.G., 2023. Arsenic and cancer: Evidence
671 and mechanisms. *Adv. Pharmacol.* 96, 151-202.
672 <https://doi.org/10.1016/bs.apha.2022.08.001>

673 Sun W., Xiao E., Hagglblom M., Krumins V., Dong Y., Sun X., Li F., Wang Q., Li B., Yan B.,
674 2018. Bacterial survival strategies in an alkaline tailing site and the physiological
675 mechanisms of dominant phylotypes as revealed by metagenomic analyses. *Environ. Sci.*
676 *Technol.* 52, 13370-13380. <https://doi.org/10.1021/acs.est.8b03853>

677 Sunagawa S., Coelho L. P., Chaffron S. *et al.*, 2015. Structure and function of the global
678 ocean microbiome. *Science* 348, 6237. <https://hal.science/hal-01233742>

679 Suting E.G. and Olivia Devi N., 2021. Occurrence and diversity of arbuscular mycorrhizal
680 fungi in trap cultures from limestone mining sites and un-mined forest soil of Mawsmai,
681 Meghalaya. *Trop. Ecol.* 62, 525-537. <https://doi.org/10.1007/s42965-021-00144-7>

682 Taleski V., Dimkić I., Boev B., Boev I., Živković S., Stanković S., 2020. Bacterial and fungal
683 diversity in the lorandite (TlAs₂) mine 'Allchar' in the Republic of North Macedonia.
684 *FEMS Microbiol. Ecol.* 96, 155. <https://doi.org/10.1093/femsec/fiaa155>

685 Torres S.B., Petrik A., Szabo K.Z., Jordan G., Yao J., Szabó C., 2018. Spatial relationship
686 between the field-measured ambient gamma dose equivalent rate and geological
687 conditions in a granitic area, Velence Hills, Hungary: an application of digital spatial
688 analysis methods. *J. Environ. Radioactiv.* 192, 267-278.
689 <https://doi.org/10.1016/j.jenvrad.2018.07.001>

690 Tuhý M., Hrstka T., Ettler V., 2020. Automated mineralogy for quantification and
691 partitioning of metal(loid)s in particulates from mining/smelting-polluted soils. *Environ.*
692 *Pollut.* 266, 115118. <https://doi.org/10.1016/j.envpol.2020.115118>

693 Umezawa K., Kojima H., Kato Y., Fukui M., 2020. Disproportionation of inorganic sulfur
694 compounds by a novel autotrophic bacterium belonging to *Nitrospirota*. *Syst. Appl.*
695 *Microbiol.* 43, 126110. <https://doi.org/10.1016/j.syapm.2020.126110>

696 Vasconcelos A.L.S., Defalco T., Dias A.C.F., Barrientos L., Bernardino A.F., Andreote F.D.,
697 Núñez-Montero K., 2021. Complete genome sequence of a *Mucilaginibacter* sp. strain
698 isolated from estuarine soil contaminated with mine tailings from the Samarco Disaster

699 at Fundão Dam. *Microbiol. Resour. Announc.* 10, e0077921.
700 <https://doi.org/10.1128/mra.00779-21>

701 Wang L., Ji B., Hu Y., Liu R., Sun W., 2017. A review on in situ phytoremediation of mine
702 tailings. *Chemosphere* 184, 594-600. <https://doi.org/10.1016/j.chemosphere.2017.06.025>

703 Wang Y., Dong R., Zhou Y., Luo X., 2019. Characteristics of groundwater discharge to river
704 and related heavy metal transportation in a mountain mining area of Dabaoshan,
705 Southern China. *Sci. Total Environ.* 679, 346-358.
706 <https://doi.org/10.1016/j.scitotenv.2019.04.273>

707 Xiao E., Krumins V., Dong Y., Xiao T., Ning Z., Xiao Q., Sun W., 2016. Microbial diversity
708 and community structure in an antimony-rich tailings dump. *Appl. Microbiol. Biotechnol.*
709 100, 7751-7763. <https://doi.org/10.1007/s00253-016-7598-1>

710 Yi X.Y., Yang Y.P., Yuan H.Y., Chen Z., Suan G., Zhu Y., 2019. Coupling metabolisms of
711 arsenic and iron with humic substances through microorganisms in paddy soil. *J. Hazard.*
712 *Mater.* 373, 591-599. <https://doi.org/10.1016/j.jhazmat.2019.03.113>

713 Yi X., Liang J., Su J., Jia P., Lu J., Zheng J., Wang Z., Feng S., Luo Z., Ai H., Liao B., Shu
714 W., Li J., Zhu Y., 2022. Globally distributed mining-impacted environments are
715 underexplored hotspots of multidrug resistance genes. *ISME J.* 16, 2099-2113.
716 <https://doi.org/10.1038/s41396-022-01258-z>

717 Zhang Y., Wang F., Hudson-Edwards K., Blake R., Zhao F., Yuan Z., Gao W., 2020.
718 Characterization of mining-related aromatic contaminants in active and abandoned
719 metal(loid) tailings ponds. *Environ. Sci. Technol.* 54, 15097-15107.
720 <https://doi.org/10.1021/acs.est.0c03368>

721 Zhu X., Yao J., Wang F., Yuan Z., Liu J., Jordan G., Šolević Knudsen T., Avdalović J., 2018.
722 Combined effects of antimony and sodium diethyldithiocarbamate on soil microbial
723 activity and speciation change of heavy metals. Implications for contaminated lands
724 hazardous material pollution in nonferrous metal mining areas. *J. Hazard. Mater.* 349,
725 160-167. <https://doi.org/10.1016/j.jhazmat.2018.01.044>

726 Zhu J., Yang K., Chen Y., Fan G., Zhang L., 2021. Revealing the substitution preference of
727 zinc in ordinary Portland cement clinker phases: a study from experiments and DFT
728 calculations. *J. Hazard. Mater.* 409, 124504.
729 <https://doi.org/10.1016/j.jhazmat.2020.124504>

730 **Figure legends**

731 **Fig. 1** SEM images of collected tailings samples, and XRD analysis of collected
732 tailings samples. a: Quartz (PDF# 46-1045), b: Manganese copper oxide
733 (PDF# 82-0668), c: Iwakiite (PDF# 38-0430), d: Celadonite (PDF# 17-0521),
734 e: Magnesium iron oxide (PDF# 77-2367).

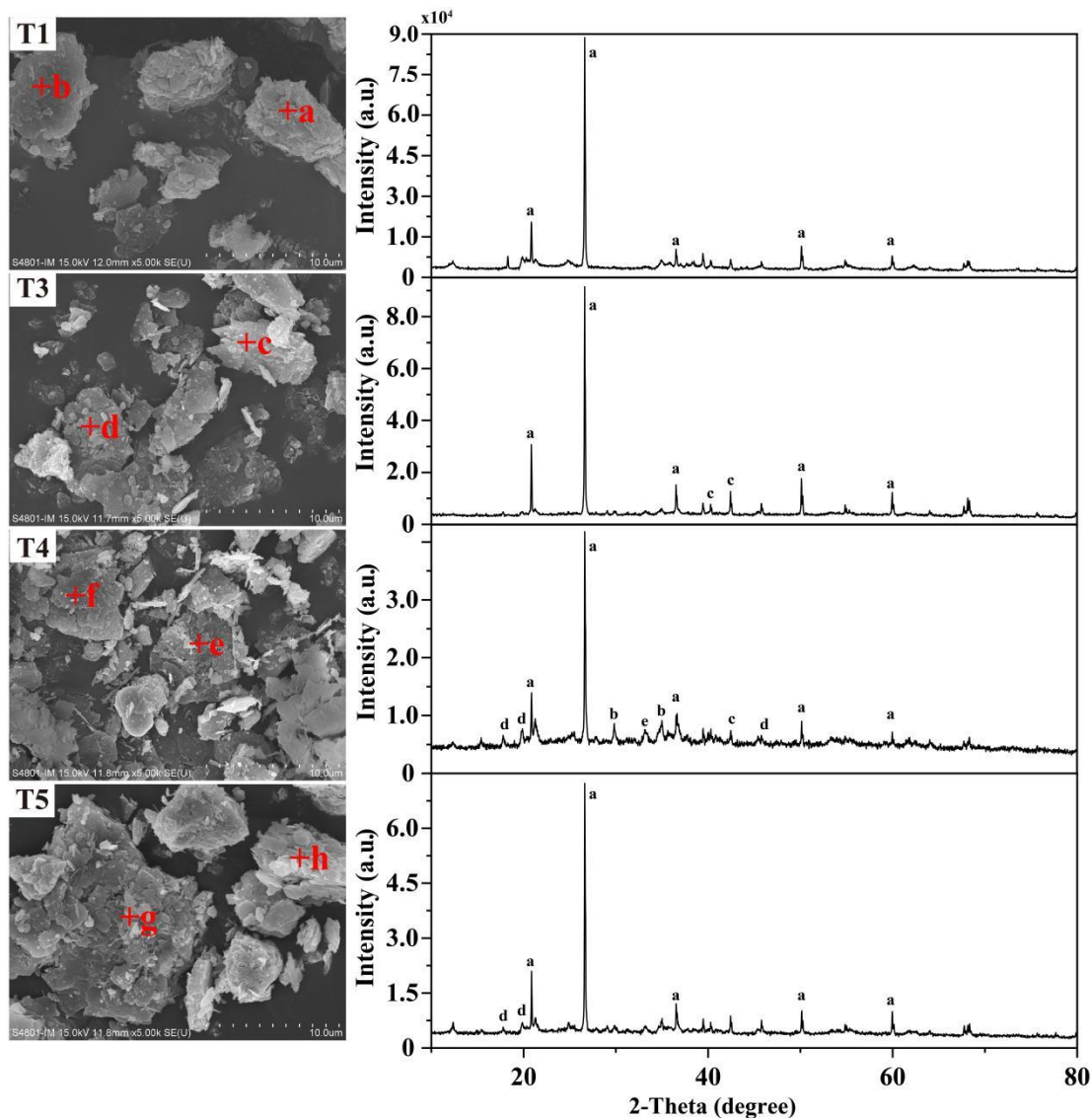
735 **Fig. 2** General patterns of microbial alpha-diversity and community assembly. (a)
736 Alpha-diversity of bacterial, fungal, and archaeal in the sampling sites.
737 Significant difference (based on the Wilcoxon test; $p \leq 0.05$). Relative
738 abundance of (b) bacterial, (c) fungal, and (d) archaeal communities. Bubble
739 sizes represent the relative abundance of the genera. The bubble color is
740 colored according to the classification information.

741 **Fig. 3** General patterns of microbial beta-diversity in studied tailings. (a-d)
742 Respective beta-diversity of bacterial, fungal, archaeal, and all taxa
743 communities based on non-metric multidimensional scaling (NMDS)
744 analysis. (e) Partial Mantel test for co-relation of three microbial groups and
745 physical-chemical parameters. A color gradient denotes the Pearson's
746 correlation coefficients.

747 **Fig. 4** Metacommunity network analysis for the detected bacterial, fungal, and
748 archaeal taxa in tailings. Each node indicates one OTU. The corresponding
749 species of each OTU was listed in Table S6. The colors of the node represent
750 the different major phyla and genera. The size of the species-node denotes
751 the abundance of species. Nodes unnamed represented the
752 no_rank/un-classified genera. The red line represents the positive correlation
753 between the two individual nodes, and the green line shows a negative
754 (exclusion) correlation.

755 **Fig. 5** (a) Variation of incidence-based (Raup-Crick) beta-diversity for microbial
756 communities. (b) Comparison of the maximum likelihood fit of the neutral
757 models estimated by the Akaike information criterion for microbial
758 communities in tailings. (c) Comparison of mean habitat niche breadths in all
759 taxa in bacterial, fungal, and archaeal communities.

760 **Fig. 6** Independent-samples *T*-test and correlation of KOs with geochemical
761 parameters. (a) Difference analysis for KOs related to metals of bacterial and
762 archaeal communities based on the independent-sample *T*-test. Data for the
763 23 shared KOs were used for analysis. * $0.01 < p \leq 0.05$, ** $0.001 < p \leq 0.01$,
764 *** $p \leq 0.001$. (b and c) Redundancy analyses (RDA) of geochemical
765 parameters (arrows) and KEGG pathways (*) of bacterial and archaeal
766 communities, respectively.



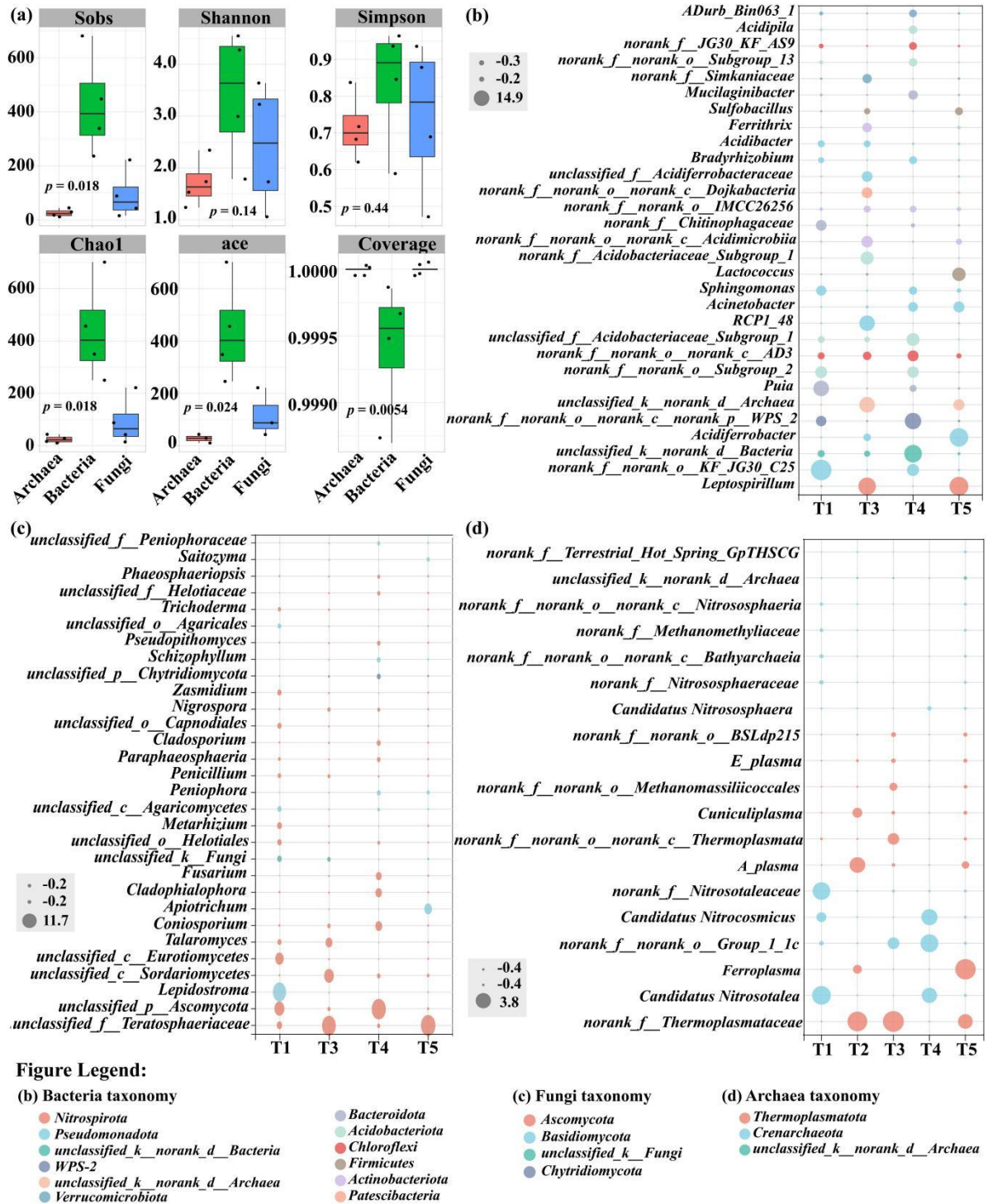
767

768 **Fig. 1** SEM images of collected tailings samples, and XRD analysis of collected

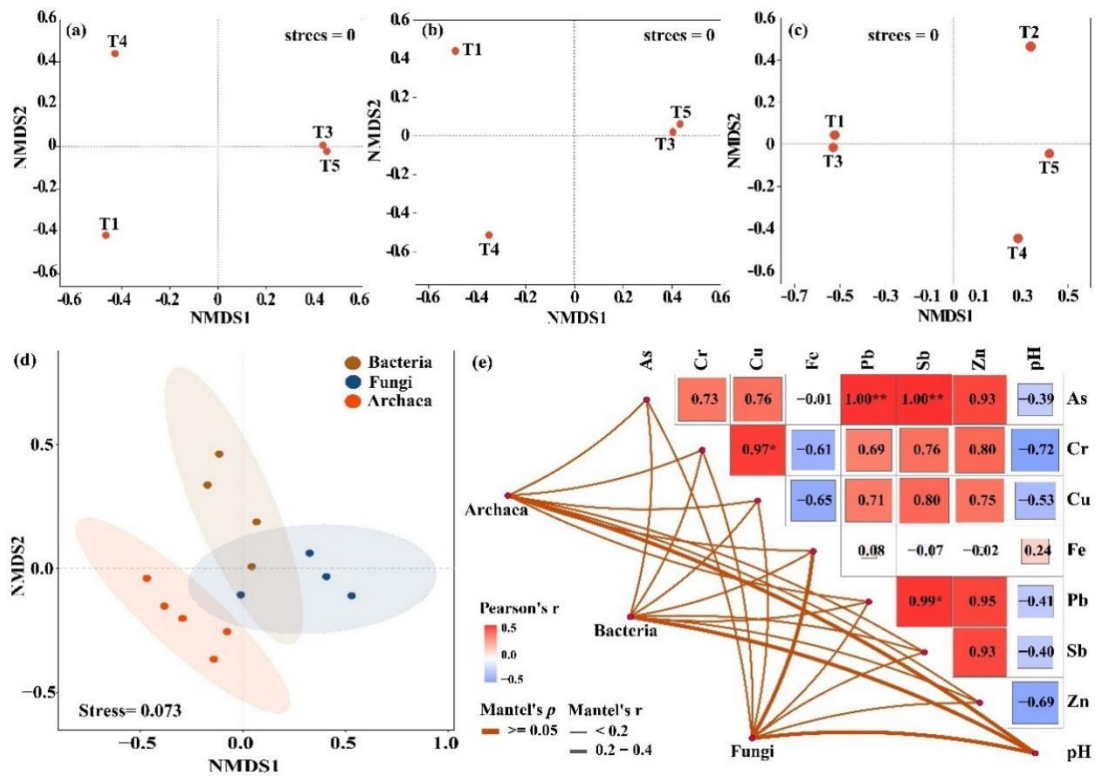
769 tailings samples. a: Quartz (PDF# 46-1045), b: Manganese copper oxide

770 (PDF# 82-0668), c: Iwakiite (PDF# 38-0430), d: Celadonite (PDF# 17-0521),

771 e: Magnesium iron oxide (PDF# 77-2367).



772 **Fig. 2** General patterns of microbial alpha-diversity and community assembly. (a)
 773 Alpha-diversity of bacterial, fungal, and archaeal in the sampling sites.
 774 Significant difference: $p \leq 0.05$ (analysis was based on the Wilcoxon test).
 775 (b-d) Relative abundance of microorganisms, corresponding to bacterial,
 776 fungal, and archaeal communities, respectively. Bubble size represented the
 777 relative abundance of the genus. The bubble color indicates the classification
 778 information.



779

780 **Fig. 3** General patterns of microbial beta-diversity in studied tailings. (a-d)

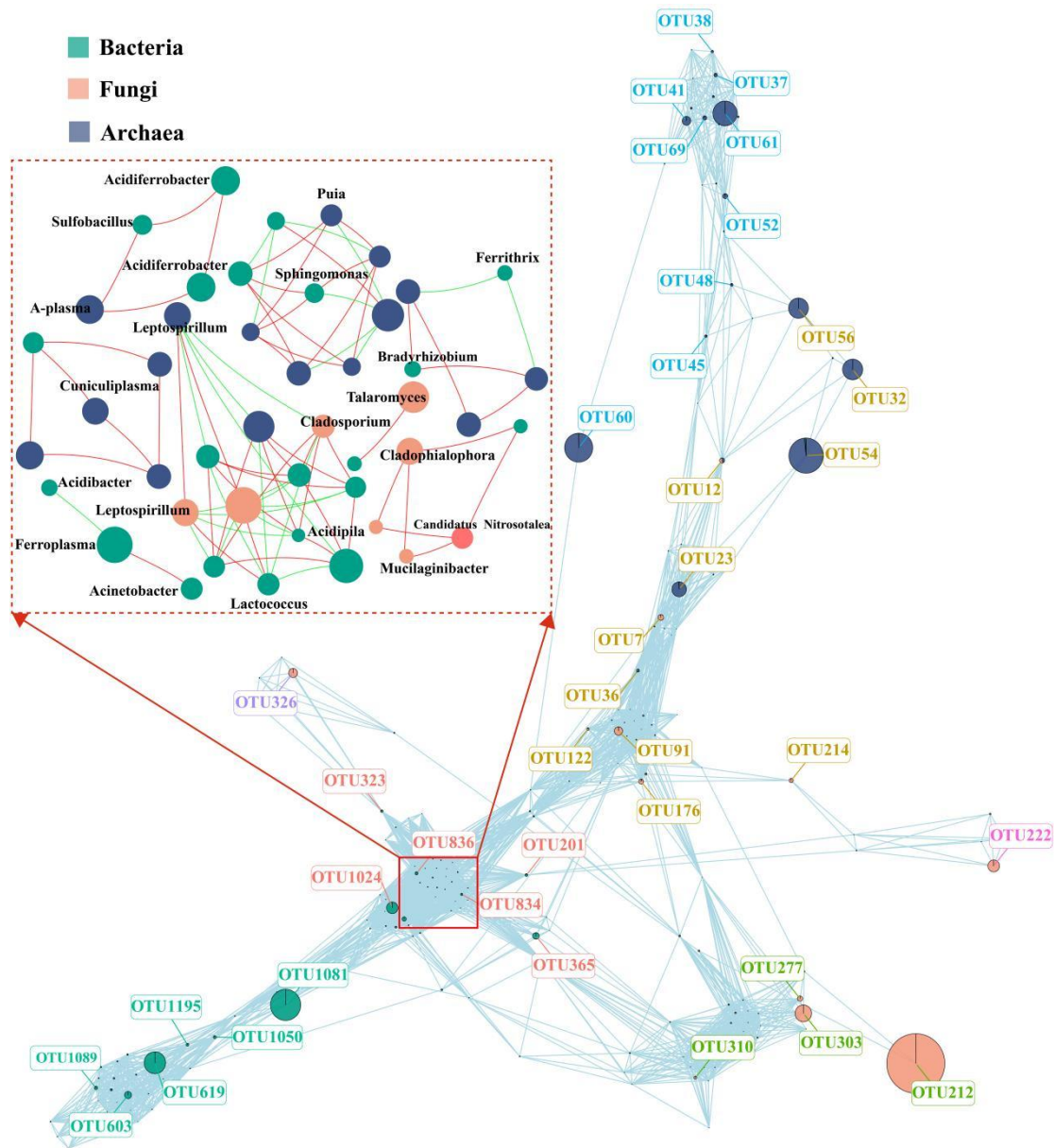
781 Beta-diversity of bacterial, fungal, archaeal, and all taxa communities based

782 on non-metric multidimensional scaling (NMDS) analysis. (e) Partial Mantel

783 test for correlation of three microbial groups and physical-chemical

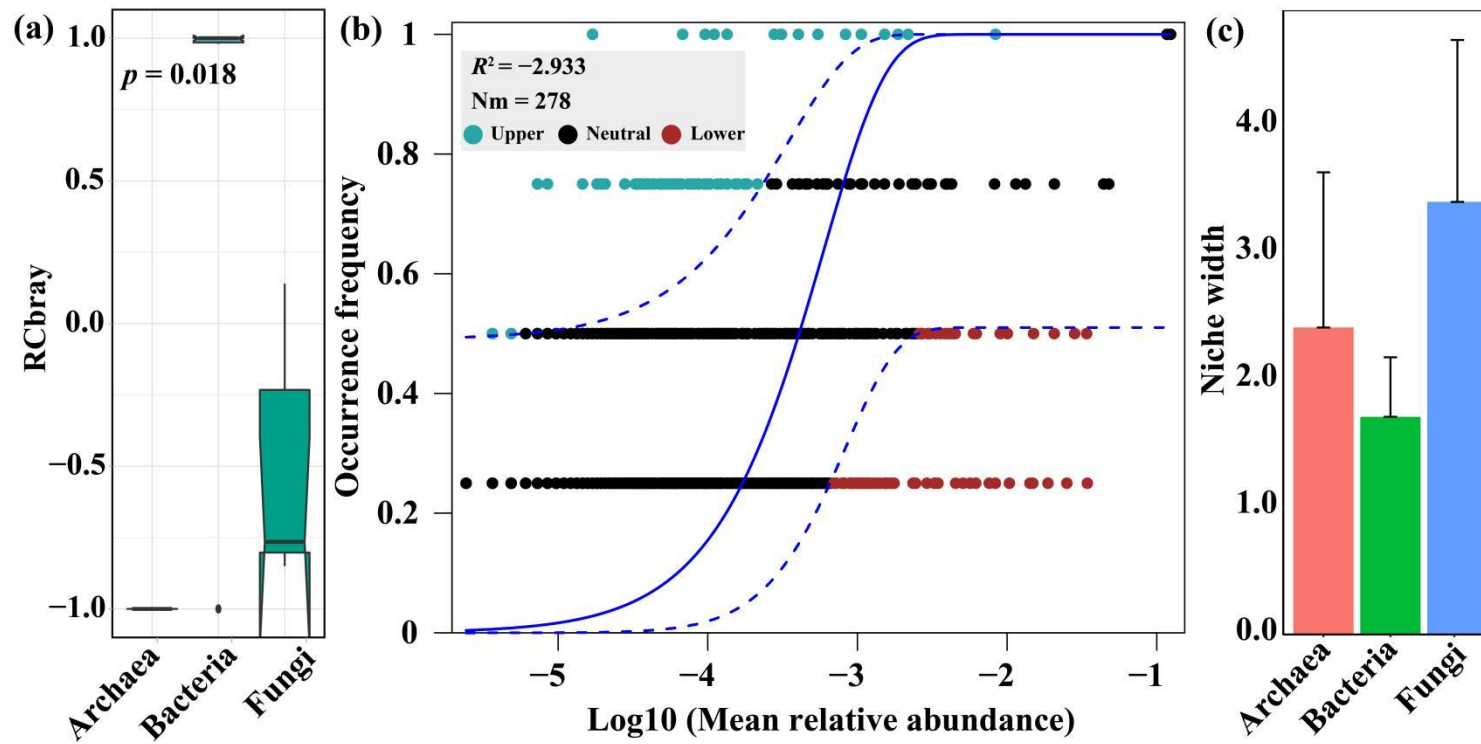
784 parameters. A color gradient denotes the Pearson's correlation coefficients.

785



786

787 **Fig. 4** Metacommunity network analysis for the detected bacterial, fungal, and
 788 archaeal taxa in tailings. Each node indicates one OTU. The corresponding
 789 species of each OTU was listed in Table S6. The colors of the nodes
 790 represent the different major phyla and genera. The size of the species-node
 791 denotes the abundance of species. Nodes unnamed represented the
 792 no_rank/un-classified genera. The red lines represent the positive
 793 correlations between the two individual nodes, the green lines show
 794 negative (exclusion) correlations.



795

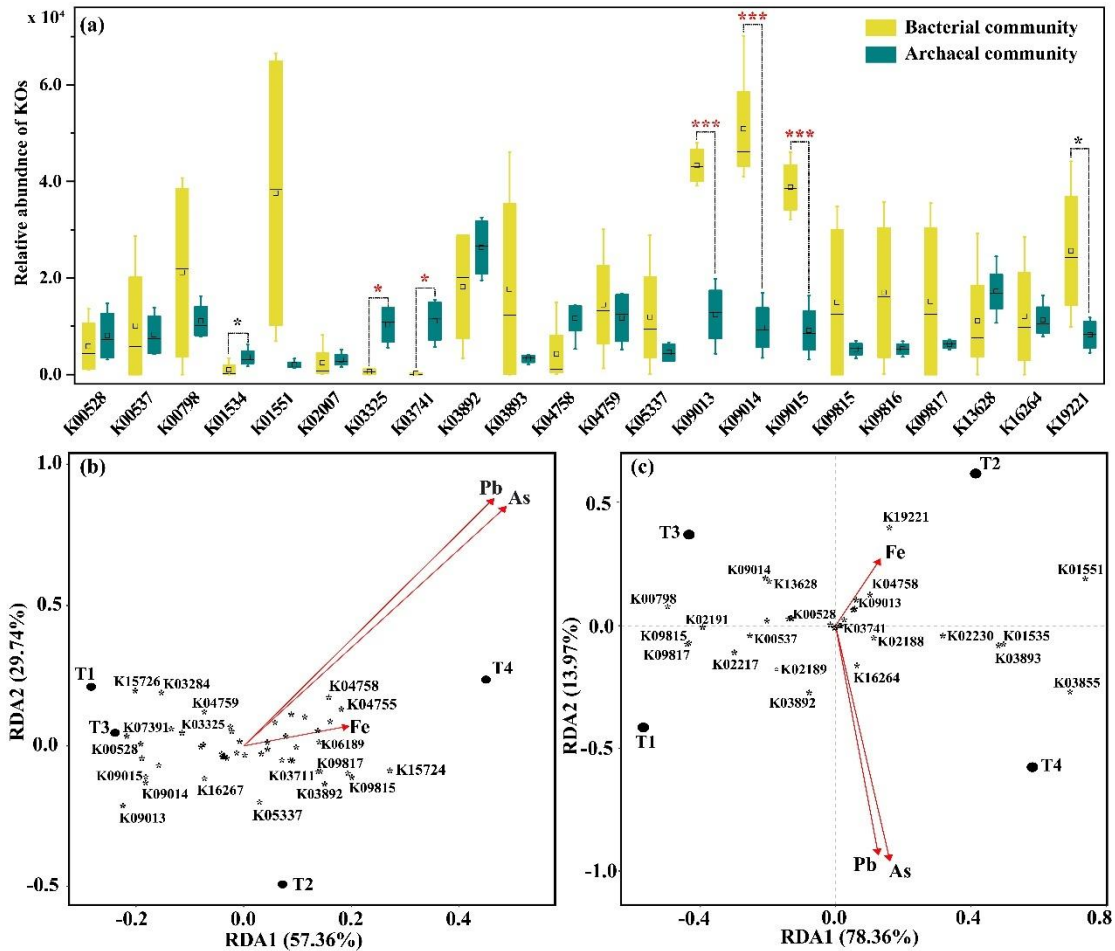
796

797

798

799

Fig. 5 (a) Variation of incidence-based (Raup-Crick) beta-diversity for microbial communities. (b) Comparison of the maximum likelihood fit of the neutral models estimated by the Akaike information criterion for microbial communities in tailings. (c) Comparison of mean habitat niche breadths in all taxa in bacterial, fungal, and archaeal communities.



800

801

Fig. 6 Independent-sample *T*-tests and correlations of KOs with geochemical

802

parameters. (a) Difference analysis for KOs related to metals of bacterial and

803

archaeal communities based on the independent-sample *T*-test. Data for the 23

804

shared KOs were used for analysis. * $0.01 < p \leq 0.05$, ** $0.001 < p \leq 0.01$, ***

805

$p \leq 0.001$. (b and c) Redundancy analysis (RDA) of geochemical parameters

806

(arrows) and KEGG pathways (*) of bacterial and archaeal communities,

807

respectively.